Discretization Accuracy of Continuous Signal Peak Values in Limited Bandwidth Systems

Luis Pastor Sánchez Fernández

Instituto Politécnico Nacional,
Centro de Investigación en Computación,
Mexico

lsanchez@cic.ipn.mx

Abstract. In many real-processes or physically modelled, the signals' peak-values must be calculated. A work's real-scale receives an amplificated impact of the small-scale measurements performed in the laboratory. Therefore, computations the maximum and minimum of the signal values have greater relevance. Likewise, other signal digital processing applications have the same behaviour. The sampling rate contributes significantly to measurement accuracy, and their effects are significant. Often, the measurement error due to the sampling frequency is not quantified. So, there are incomplete measurement specifications. There are no understandable formulations to obtain the possible highest errors due to the continuous signals' discretization, especially when the system bandwidth is limited. This paper presents a comprehensive general analysis based on the relation between the sampling frequency and the highest measurement error for a sinusoidal signal. The relative maximum (highest) errors on the peak values are calculated, with understandable mathematical expressions. Computations of peak-values' relative maximum errors for post-processing mode have more details by its increased use. Additionally, analyses for signals composited of several harmonics, such as biomechanical signals and waves in hydraulic research laboratories, have specific examples in this paper. Some case studies analyze cubic spline interpolation effects.

Keywords. Discretization accuracy, signal peak values, sampling frequency, measurement errors.

1 Introduction

The continuous signals discretization must meet accuracy specifications; these are often ignored. The sampling frequency is essential; the well-known sampling theorem is fundamental, but not sufficient. These specifications are very remarkable in calculating the signal peak-values; mainly when the research is conducted on a small-scale. Therefore, the acquired digital information quality is an essential descriptor for all measurement and control systems.

It is desirable to choose a sampling frequency that does not represent a heavy burden for the data acquisition system. In many applications, this sampling rate implies an efficient use of the central processing unit or data acquisition hardware. On the other hand, the sampling rate to acquire, save and transmit less information can be reduced and then interpolate in the receiver [1].

Shannon's sampling theorem [2, 3] establishes the minimum angular sampling frequency W_s to reconstruct a limited bandwidth continuous signal $X(t)$ based on the samples taken in T period: $W_s = 2\pi/T$; where W_s is radians/second; T is the sampling period in seconds.

For instance, a sinusoidal signal $X(t) = Asin(wt)$; where w is the angular frequency of the $X(t)$ signal; If W_s is greater or equal than $2w$, then $X(t)$ can be reconstructed based on the samples taken. However, this well-known theorem and many publications have not formulated or presented the recommended sampling frequency for applications with specific requirements.

For the abovementioned, mathematical expressions are necessary for a relationship between the sampling rate and the measurement accuracy. However, there are some practical criteria. For instance, for control systems, the sampling frequency should be based on knowledge of their characteristics. Thus, it is reasonable to consider the closed-loop control

system bandwidth, or the rising time [4]. A good selection takes the sampling frequency between 10 and 20 times greater than the bandwidth.

Automatic control systems have dynamic characteristics of low-pass filters, allowing a relatively low sampling frequency, among other aspects of their designs [5]. The relations abovementioned can be small for typical signal processing applications [1, 6], [7].

A practical criterion for sea wave [8, 9] is to consider the signal spectrum peak frequency (f_p), and choosing the sampling frequency f_s according to the following relationship: $f_s \geq 8f_p$. This criterion is recommended for measuring and irregular-wave generation systems in research laboratories [9]. Where f_s has been used to denote the sampling frequency in Hertz (Hz) or samples per second.

All the above cases are based on practical criteria guaranteeing an acceptable accuracy depending on the application type. However, when an application should not increase the computational cost in real-time or the data acquisition card does not allow a higher data sampling rate, there are other solutions.

For example, If the application provides post-processing of collected data, several methods can be applied to reduce sampling frequency's adverse effect without increasing it so much. This paper intends to be useful for the academy, researchers and industry. It is possible to calculate the maximum error due to sampling frequency based on mathematical expressions. A comprehensive general analysis is developed based on the relation between the sampling frequency and the maximum measurement error for a sinusoidal signal. The harmonic of greater amplitude is relevant in many applications and computation types [10–24].

As mentioned previously, the sinusoidal signals type is the basis for finding the proposed formulations by this paper in Section 2. Besides, they have been used in various applications developed successfully for several years. Those mathematical expressions are useful in signals with several harmonics if their objective-bandwidth is well-thought-out; or otherwise, those that have some significant harmonics. In this sense, Section 4 will analyze several experimental examples where the previous statements are true.
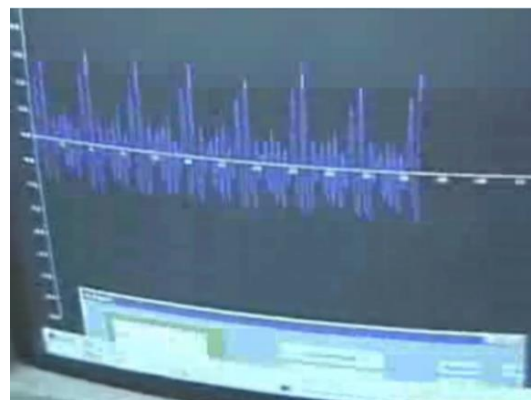
Fig. 1. Wave research laboratory for maritime and coastal works designs: a) Rectangular section measuring channel; b) Signals with relevant peak-values

The paper's remainder has several sections: Review; Material and Methods; Experimentations and Results, which present signals for a wave generation hydraulic channel and biomechanical signal measurements in Parkinson disease patients; Discussion and Conclusions.

2 Review

A physically modelled process, such as a wave research laboratory for maritime and coastal works design, requires calculating the signals' peak values [8, 9, 22, 25], as Fig. 1 shows.

Assessments use small-scale models, and their computations are transformed into real-scales,

finally. Maximum errors must be calculated with high accuracy in the laboratory to know and evaluate their real-works impacts.

Similar situations occur in the design of mechanical systems [26]. In other measurement systems, for example, in biomechanical assessments, the multiple freedom degrees of their triaxial signals and wireless communication bandwidth limitations may not allow increasing the sampling rate, as shown in Fig. 2. In these cases, signals' peak-values computations are relevant. This known behaviour enables us to give the appropriate treatment to acquired signals and obtain good results in the advanced digital signals processing and when artificial intelligence methods are used [18–21, 27].

2 Material and Methods

2.1 Measurement Accuracy and Sampling Frequency

This section presents several analyzes and examples that improve understanding of the relationship between sampling frequency and measurement accuracy for signals composited of several harmonics. This analysis is based on the bandwidth and the error expressions for a sinusoidal signal, in real-time and post-processing mode, which is useful when a designer must present with absolute certainty the accuracy specifications of a measurement system being very relevant when the signal peak-values are calculated.

2.2 Data Post-Processing Mode

Real-time calculations are not necessary for many applications. Instead, these computations can be made on data previously acquired (post-processing mode) to calculate the maximum and minimum signal values. Fig. 3. Presents the absolute maximum error due to sampling frequency during the peak-value calculation ($E_{pabs(POS)}$) for a sinusoidal signal.

Where $E_{pabs(POS)}$ is the absolute maximum error during the peak-value computation in post-processing mode. Where *x(k), x(k+1)* is the signal value in $t = kT$ and $t = (k+1)T$, respectively, *T:*
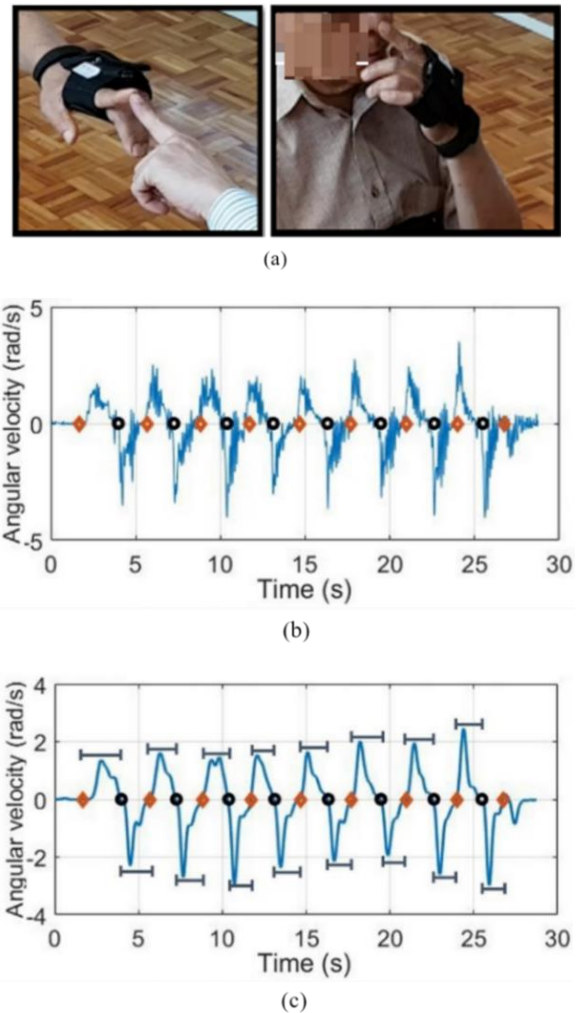

(a)

(b)

(c)

Fig. 2. a) Parkinson disease patient during a finger to nose exercise and signal of the gyroscope X-axis; b) Raw signal (low and high-frequency components; c) Filtered signal (only low-frequency components) with relevant pick values

sampling period and *k* is an integer value *(k=1,2,3,.....)*. Absolute maximum error of peak-value, in post-processing mode $E_{pabs(POS)}$ occurs when none of the values of the samples taken coincides with the signal peak-value. This error will be the maximum when the samples' arrangement presented in Fig.3 are equidistant from the peak-value:

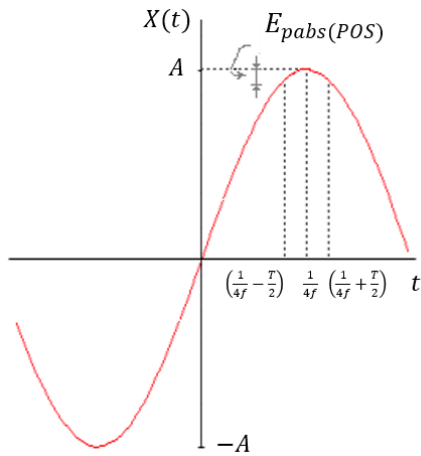$$E_{pabs(POS)} = |X(k + 0.5) - X(k)|, \qquad (1)$$

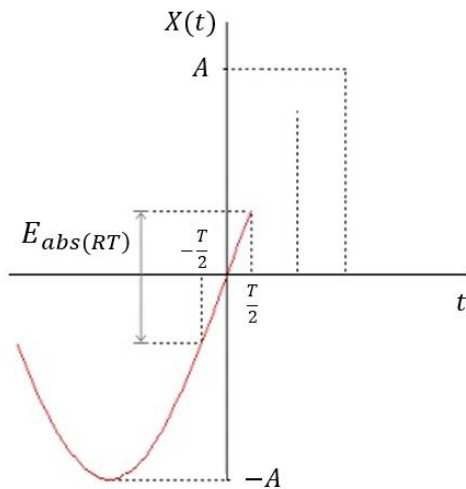**Fig. 3.** Absolute maximum error during the calculation of peak value in post-processing mode

Fig. 4. The absolute maximum error in real-time measurements for a sinusoidal signal with frequency *f*

$$X(k + 0.5) = Asin(2\pi f\, 1/4f), \tag{2}$$

$$X(k + 0.5) = Asin(\pi/2) = A, \tag{3}$$

$$X(k) = Asin[(2\pi f\, 1/4f - T/2)], \tag{4}$$

$$X(k) = Asin\left[2\pi f\left(\frac{1 - 2fT}{4f}\right)\right] = Asin\left[\frac{\pi}{2}(1 - 2fT)\right]. \tag{5}$$

Replacing $T = \frac{1}{F_s} = \frac{1}{nf}$; the expression (5) will become (6):

$$X(k) = Asin\left[\frac{\pi}{2}\left(1 - 2f\frac{1}{nf}\right)\right], \tag{6}$$

$$X(k) = Asin\left(\frac{\pi}{2} - \frac{\pi}{n}\right) = Acos\left(\frac{\pi}{n}\right), \tag{7}$$

$$E_{pabs(POS)} = A\text{-}Acos\left(\frac{\pi}{n}\right), \tag{8}$$

The relative maximum error $(E_{prel(POS)})$ regarding the peak-to-peak signal value expressed in per cent will be formulated with Eq. (10):

$$E_{prel(POS)} = \frac{A - Acos\left(\frac{\pi}{n}\right)}{2A}x100, \tag{9}$$

$$E_{prel(POS)} = 0.5\left[1 - cos\left(\frac{\pi}{n}\right)\right]x100. \tag{10}$$

2.3 Real-Time Processing Mode

The absolute maximum error in real-time is located symmetrically to coordinate axis origin, where the highest signal change speed occurs, as shown in Fig. 4. The maximum error is calculated using a zero-order hold. Therefore, a signal sample remains valid until the next sample is taken (next sampling period):

$$E_{abs(RT)} = Max\,|X(k + 1) - X(k)|. \tag{11}$$

where $E_{abs(RT)}$ is the absolute maximum error in real-time; $X(k + 1)$, $X(k)$ is the signal value at $t = (k + 1)T$ and $t = kT$, respectively; *T* is the sampling period, and k is an integer value:

$$X(k + 1) = Asin(2\pi f\, T/2), \tag{12}$$

$$X(k) = Asin[2\pi f(-T/2)], \tag{13}$$

$$E_{abs(RT)} = |Asin(2\pi f\, T/2) - Asin[2\pi f(-T/2)]|, \tag{14}$$

$$E_{abs(RT)} = |2Asin(2\pi f\, T/2)|, \tag{15}$$
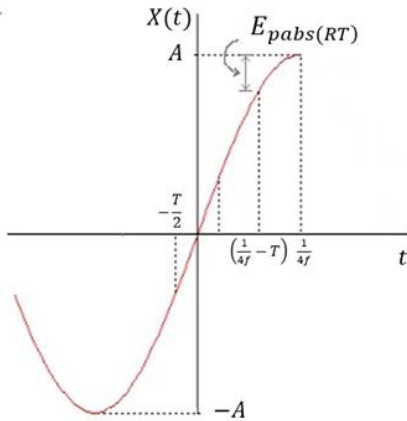
$$E_{abs(RT)} = 2A|sin(\pi fT)|$$

Fig. 5. The absolute maximum error produced around the peak values in real-time processing mode ($E_{pabs(RT)}$) for a sinusoidal signal
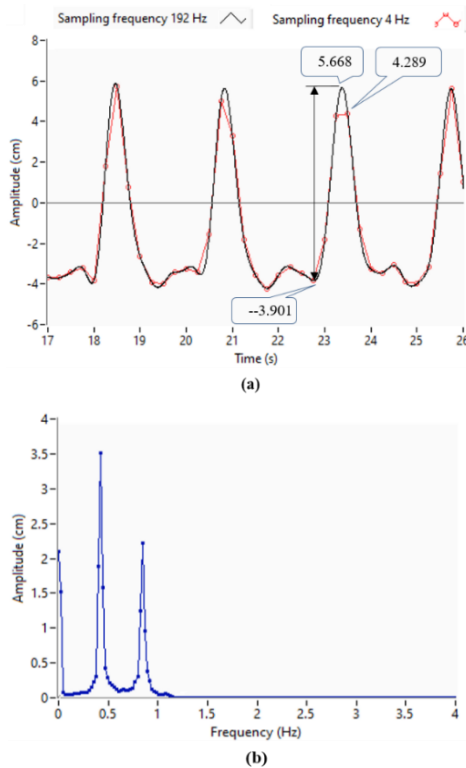

Fig. 6. A typical signal for a wave generation hydraulic channel: a) The time-domain signal with 192 Hz and 4 Hz sampling frequency; b) The frequency domain signal sampled at 192 samples per second. The highest frequency harmonic is 1.1 Hz

$$= 1/F_s T, \tag{16}$$

where F_s is the sampling frequency; making $F_s = nf$, where f is the sinusoidal signal frequency and n is an integer greater or equal to two; the resulting is the Eq. (17):

$$E_{abs(RT)} = 2A sin(\pi/n). \tag{17}$$

The maximum relative error in real-time ($E_{rel(RT)}$) regarding the signal's peak-to-peak value, expressed in per cent will be formulated with Eq. (19).

$$E_{rel(RT)} = \frac{2A sin(\pi/n)}{2A} x100, \tag{18}$$

$$E_{rel(RT)} = sin(\pi/n)\, x100, \tag{19}$$

Fig. 5 shows the illustration of the absolute maximum error produced around the peak values in real-time processing mode ($E_{pabs(RT)}$**)**, which is based on Eqs. (20) to (28):

$$X(k+1) = A sin(2\pi f\, 1/4f) = \\ A sin(\pi/2) = A, \tag{20}$$

$$X(k) = A sin[\, 2\pi f\, (1/4f - T\,)], \tag{21}$$

$$X(k) = A sin\left[2\pi f\left(\frac{1-4fT}{4f}\right)\right], \tag{22}$$

$$X(k) = A sin\left[\frac{\pi}{2}(1-4fT)\right]. \tag{23}$$

The sampling period can be written as $T = \frac{1}{nf}$ obtaining the Eq. (24):

$$X(k) = A sin\left[\frac{\pi}{2}\left(1-4f\frac{1}{nf}\right)\right], \tag{24}$$

$$X(k) = A sin\left(\frac{\pi}{2}-\frac{2\pi}{n}\right) = A cos\left(\frac{2\pi}{n}\right), \tag{25}$$

$$E_{pabs(RT)} = A - A cos\left(\frac{2\pi}{n}\right). \tag{26}$$

Equation (27) shows the relative maximum error in real-time, regarding the peak-to-peak of signal value ($E_{prel(RT)}$) in per cent:

$$E_{prel(RT)} = \frac{A - A cos\left(\frac{2\pi}{n}\right)}{2A} x 100, \qquad (27)$$

$$E_{prel(RT)} = 0.5\left[1 - cos\left(\frac{2\pi}{n}\right)\right] x 100. \qquad (28)$$

Table 1 presents the results of the evaluation of the Eqs. (10), (19) and (28) for several sampling frequencies, being n multiples of the sinusoidal signal frequency.

3 Experimentations and Results

3.1 Wave Generation Hydraulic Channel

Fig. 6 presents a typical signal for a wave generation hydraulic channel used at physical modelling on time and frequency domains, in post-processing mode for a segment between 17 to 26 seconds. This signal harmonics are less than 1.1 Hz, and it was sampled at 192 and 4 samples per second, simultaneously. There is a significant loss of information around the maximum peak value with a sampling frequency of 4 Hz. Nevertheless, the maximum error during the peak-value calculation in post-processing mode has not occurred because the red signal points are not equidistant from the peak-value. If the sampling frequency of 192 Hz is considered as reference, Eqs. (20) and (30) present the relative error ($e_{prel(POS)}$) produced around the peak-values in post-processing mode, in per cent. In maritime hydraulics for small-scale physical modelling, those errors are substantial.

In this example, the behaviour was less severe because there is only an error during the maximum peak computation and one sample coincided with the minimum peak. Eq. (30) presents the relative error produced around the peak value in post-processing mode, in per cent, for a signal segment between 22 and 24 seconds:

$$e_{prel(POS)} = \frac{(5.668 - 4.289)}{(5.668 - (-3.901))} = 0.1441, \qquad (29)$$

Table 1. Relative errors and sampling frequency

n	$E_{prel(POS)}\%$ Eq. (10)	$E_{prel(RT)}\%$ Eq. (28)	$E_{rel(RT)}\%$ Eq.(19)
2	50	100	100
4	14.64	50	70.71
8	3.8	14.64	38.26
10	2.44	9.54	30.9
20	0.61	2.44	15.64
50	0.098	0.39	6.27
100	0.024	0.098	3.14
200	0.0061	0.024	1.57
300	0.0027	0.0109	1.04

$E_{prel(POS)}$: *relative maximum error around the peak-values in post-processing mode.* $E_{prel(RT)}$: *relative maximum error in real-time around the peak-values.* $E_{rel(RT)}$: *maximum relative error in real-time*

$$e_{prel(POS)} = 14.41\%. \qquad (30)$$

The relative maximum error ($E_{prel(POS)}$) produced around the peak-values in post-processing mode based on Eq. (10) is 17.53%, considering the highest frequency harmonic equal to 1.1 Hz (view Fig. 6b).

3.2 Biomechanical Signal Measurement in Parkinson Disease Patients

In this application, the hardware and communication devices are not allowed to use a higher sampling frequency. The three inertial measurement units with nine degrees of freedom (accelerometer, gyroscope and magnetometer tri-axial) are connected to a computer by Bluetooth, and there is limited bandwidth.

Fig. 7 presents a left-hand postural tremor of a Parkinson disease patient with a sampling frequency of 50 Hz (50 samples per second). Fig. 7c shows the peak amplitude spectrum. This signal has been sampled five times concerning the highest-frequency harmonic, which is 10 Hz. Based on Eq. (10), the relative maximum error

$E_{prel(POS)}$ produced around the peak values is 9.55%.

Fig. 8 presents a signal section of Fig. 7b from 31.5 to 32 seconds with a sampling frequency of 300 Hz (reference) and 50 Hz, respectively (simultaneous sampling) with test hardware. Eq. (32) presents a relative error produced around the peak value in post-processing mode in per cent for the segment mentioned above.

$$e_{prel(POS)} = \frac{(0.3-0.25)}{(0.3-(-0.3))} = 0.0833, \qquad (31)$$

$$e_{prel(POS)} = 8.33\%, \qquad (32)$$

Based on Eq. (10) the relative maximum error $E_{prel(POS)}$ produced around the peak values would be 9.55%.

The relative error $e_{prel(POS)}$ produced around the peak-value in post-processing mode (8.33%) is less than the relative maximum error $E_{prel(POS)}$ (9.55%) for 50 Hz, which is five times the objective signal bandwidth but it's a close-value. In other signal examples, the results are similar.

A measurement system's maximum error specification means that the measurement error will not be greater than the worst-case scenario's specified maximum error. In the examples shown, that statement is true. In numerous cases analyzed, the behaviour is similar, and it can be stated that the formulations proposed have a very favourable practical value.

4. Discussion

Eqs. (10), (19) and (28) present the relative errors according to the sampling frequency for a sinusoidal signal. However, for composed signals of several harmonics can be considered its bandwidth or the highest-frequency harmonic. In other words, the frequency range in which most of the signal power is concentrated. For example, in Fig. 7c the harmonics with frequencies greater than 10 have very small amplitudes and minimum energy. For instance, in Fig. 7c the harmonics with frequencies greater than 10 have very small amplitudes and therefore, a minimum power.
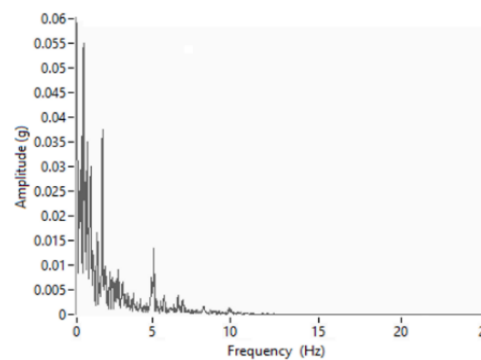
The Eq. (10) is useful because the relative error $e_{prel(POS)}$ obtained with Eq. (30) and Eq. (32)
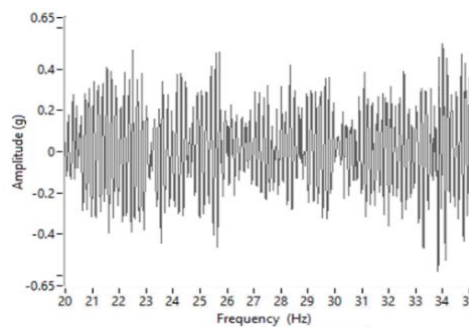
Fig. 7. A left-hand postural tremor: (a) A Parkinson disease patient; (b) Y-axis signal of the accelerometer; (c) Magnitude spectral (peak). The highest frequency-harmonic is 10 Hz

always will be less than or equal to maximum error. Similar results are obtained for other signal examples with several sampling frequencies.

In many cases, when hardware limitations do not allow increasing the sampling frequency, the cubic spline interpolation is a good option [18, 21]. In several applications, a practical criterion is to use an interpolation factor from 5 to 10. Interpolation factor greater than ten does not offer

appreciable improvements. Fig. 9a presents a signal section of Fig. 7b with a sampling frequency of 50 Hz, with cubic spline interpolation factor equal to 1 (equivalent sample rate of 100 Hz) for a time interval from 11.5 to 12 seconds. Fig 10b another time interval from 33.5 to 34 seconds. In both cases, the cubic spline interpolation effect enables greater accuracy in peak-values calculations, decreasing the error due to the sampling frequency.

4.1 Comparison with some Works more Closely Related

Often, measurement errors due to the sampling frequency are not quantified. If not possible to increase the sampling frequency, some methods to reduce its effect on the measurement accuracy must be used. Generally, few works analyze in a practical way or present mathematical expressions of the error due to the sampling rate, especially in peak-values calculations. This section presents a comparison with some work more closely related.

Paper [22] only evaluates the measurement error in wave research laboratories, fundamentally, based on a sinusoidal signal. That work presents one graph of the cubic spline interpolation and does not quantify its effect on the raw signal.

The paper [28] examines the impact of digital processing, and discretization or sampling of sea surface elevations. The theory of random linear waves, the probability distributions for the measured wave heights and amplitudes have been obtained as conditional for the sampling frequency. Rates of 1 Hz or less may lead to significant underestimation of the probability of huge waves.

In [29] and [25] the relationship between the sampling frequency and measurement's maximum error is obtained for continuous sinusoidal signals The data are processed using the Fast Fourier Transform (FFT) and interpolation of cubic splines. Graphical and statistical examples are shown for a wave research laboratory.

The paper [30] presents the phase-locked spikes in various types of neurons encode temporal information. The metric called vector strength (VS) quantifies the degree of phase-locking. In electrophysiological experiments, the timing of an action potential is detected with finite
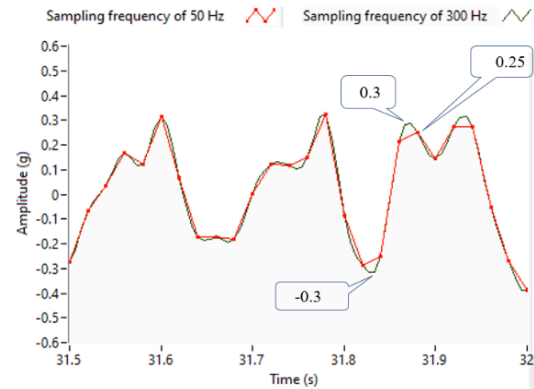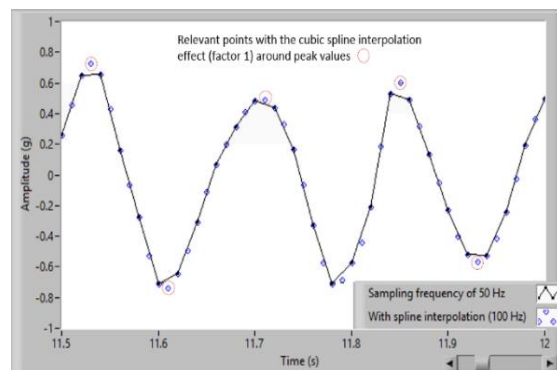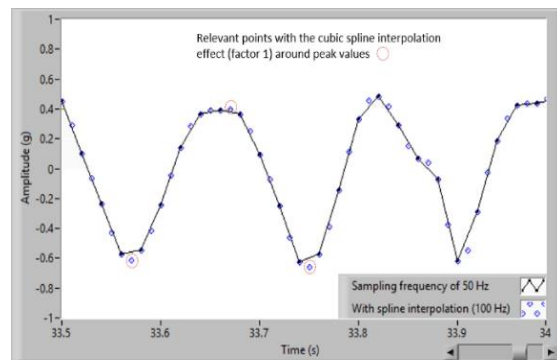

Fig. 8. A signal section of Fig. 7 from 31.5 to 32 seconds and peak values

Fig. 9. A signal section of Fig. 7b with a sampling frequency of 50 Hz, with cubic spline interpolation factor equal to 1 (equivalent sample rate of 100 Hz); a) A time interval from 31.5 to 32 seconds; b) Another time interval from 33.5 to 34 seconds

temporal precision, which is determined by the sampling frequency. The errors in VS, assuming

random sampling effects will be estimated. The impacts of analogue-to-digital conversion (ADC) quantization noise on the recovery of harmonic amplitudes and phases in the presence of large fundamental amplitudes are examined by theory and simulation [30], to determine the noise limits of instrumentation system design for power systems monitoring and harmonic power-flow measurement.

In this paper, a comprehensive analysis is developed based on the relation between the sampling frequency and the maximum measurement error for a sinusoidal signal. The real-time processing mode presents mathematical expressions of relative maximum errors around the peak-values. The relative maximum error of peak-values calculation in post-processing mode is analyzed with more relevance. Additionally, signals composited of several harmonics have some illustrative examples.

Biomechanical signals and research laboratories waves are objectives of this work as interesting examples. The error due to sampling frequency is quantified in a material very understandable. Some examples evaluate the cubic spline interpolation and its effects. Besides, the general analysis is useful for any signal where the peak-values computation represents the main aim. For many years, the research group has used these design criteria to evaluate several data acquisition systems' performance based on sampling frequency. For examples, for wave research and hydraulic laboratories [23, 31]; environmental noise in urban areas and airports [12–16]; biomechanical signal analyzes [18–21, 32]; and fault diagnose based on mechanical vibrations [33, 34].

5 Conclusions

The Eq. (10) allows calculating the relative maximum error produced around the peak-values in post-processing mode. Eq. (19) computations the relative maximum error in real-time. Likewise, Eq. (28) is the representations of the error around the peak-values also in real-time. These three equations have utility in signals with several harmonics if their objective-bandwidth is well-thought-out; or otherwise, signals that have some significant harmonics. Many applications have demonstrated the usefulness of these design criteria to evaluate the data acquisition systems' performance. These equations permit to quantify the measurement accuracy based on sampling frequency. The error by samples rate always will be less than the maximum error computed by these equations. The maximum relative mistake during the peak-values calculation in post-processing mode is analyzed with more relevance because it is widely used in many engineering areas.

The cubic splines interpolation, widely mentioned and well-accepted by many authors and available in signal-processing commercial software, reconstructs the time-series adding intermediate points, *producing an effect that could be considered similar at a higher sample rate*. A practical criterion in several applications is to use an interpolation factor from 5 to 10. In general, the interpolation factor greater than ten does not offer appreciable improvements.

Acknowledgements

References

1. **Oppenheim, A. (1997).** Signals & Systems. Prentice-Hall.

2. **Shannon, C.E. (1948).** A mathematical theory of communication. The Bell System Technical Journal, Vol. 27, No. 3, pp. 379–423. DOI: 10.1002/j.1538-7305.1948.tb01338.x.

3. **Shannon, C.E. (1949).** Communication in the presence of noise. Proc IRE, Vol. 37, pp. 10–21.

4. **Ogata, K., Columbus, B., New, I. (2010).** Modern Control Engineering.

5. **Oppenheim, A.V., Schafer, R.W (2014).** Discrete-time signal processing. Pearson.

6. **Proakis, J.G, Manolakis, D.G. (2007).** Digital signal processing. Pearson Prentice Hall.

7. **Åström, K.J., Karl, J., Wittenmark, B. (2011).** Computer-controlled systems : theory and design. Dover Publications.

8. **Goda, Y (2010).** Random seas and design of maritime structures. World Scientific.

9. **Beresford, P.J. (1994).** WAVEGEN-Wave generator control software program.

10. **Sanchez-Perez, L.A, Sanchez-Fernandez, L.P., Suarez-Guerra, S., Lopez-Pacheco, M.G. (2015).** Dynamic hierarchical aggregation of parallel outputs for aircraft take-off noise identification. Eng. Appl. Artif. Intell., Vol. 46, Part A, pp. 33–42. DOI: 0.1016/j.engappai.2015.08.002.

11. **Sanchez-Perez, L.A., Sanchez-Fernandez L.P., Shaout, A., Suarez-Guerra, S. (2016).** Airport take-off noise assessment aimed at identify responsible aircraft classes. Sci Total Environ, Vol. 542, pp. 562–577. DOI: 10.1016/j.scitotenv.2015. 10.037.

12. **Sánchez-Fernández, L.P., Sánchez-Pérez, L.A., Carbajal-Hernández, J.J., Rojo-Ruiz, A. (2013).** Aircraft classification and acoustic impact estimation based on real-time take-off noise measurements. Neural Process Lett, Vol. 38, pp. 239–259. DOI: 10.1007/s11063-012-9258-5.

13. **Sánchez-Pérez, L.A., Sánchez-Fernández, L.P., Suárez-Guerra, S., Carbajal-Hernández, J.J. (2013).** Aircraft class identification based on take-off noise signal segmentation in time. Expert. Syst. Appl., Vol. 40, No. 13, pp. 5148–5159. DOI: 10.1016/ j.eswa.2013.03.017.

14. **López-Pacheco, M.G., Sánchez-Fernández, L.P., Molina-Lozano, H. (2014).** A method for environmental acoustic analysis improvement based on individual evaluation of common sources in urban areas. Science of The Total Environment, Vol. 468–469, pp. 724–737. DOI: 10.1016/ j.scitotenv.2013.08.085.

15. **Márquez-Molina, M., Sánchez-Fernández, L.P., Suárez-Guerra, S,. Sánchez-Pérez, L.A. (2014).** Aircraft take-off noises classification based on human auditory's matched features extraction. Appl Acoust, Vol. 84, pp. 83–90. DOI: 10.1016/ j.apacoust.2013.12.003.

16. **Sánchez-Pérez, L.A., Sánchez-Fernández, L.P., Suárez-Guerra, S., Márquez-Molina, M. (2014).** Geo-referenced flight path estimation based on spatio-temporal information extracted from aircraft take-off noise. Digit Signal Process A Rev. J., Vol. 30, pp. 1–14. DOI: 10.1016/j.dsp.2014.03.004.

17. **Flores-Carrillo, D.A., Sánchez-Fernández, L.P., Sánchez-Pérez, L.A., Carbajal-Hernández, J.J. (2017).** Soil moisture Fuzzy Estimation Approach based on Decision-Making. Environ. Model. Softw., Vol. 91, pp. 223–240. DOI: 10.1016/j.envsoft. 2017.01.018.

18. **Ornelas-Vences, C., Sanchez-Fernandez, L.P., Sanchez-Perez, L.A. (2017).** Fuzzy inference model evaluating turn for Parkinson's disease patients. Comput. Biol. Med., Vol. 89, No. 11, pp. 379–388. DOI: 10.1016/j.compbiomed.2017.08. 026.

19. **Garza-Rodríguez, A., Sánchez-Fernández, L.P., Sánchez-Pérez, L.A., (2018).** Pronation and supination analysis based on biomechanical signals from Parkinson's disease patients. Artif. Intell. Med. Vol. 84, pp. 7–22. DOI: 10.1016/j.artmed.2017. 10.001.

20. **Sanchez-Perez, L.A., Sanchez-Fernandez, L.P, Shaout, A. (2018).** Rest tremor quantification based on fuzzy inference systems and wearable sensors. Int. J. Med. Inform., Vol. 114, pp. 6–17. DOI: 10.1016/j.ijmedinf.2018.03.002.

21. **Ornelas-Vences, C., Sánchez-Fernández, L.P., Sánchez-Pérez, L.A., Martínez-Hernández, J.M. (2019).** Computer model for leg agility quantification and assessment for Parkinson's disease patients. Med. Biol. Eng. Comput., Vol. 57, 463–476. DOI: 10.1007/s11517-018-1894-0.

22. **Sánchez-Fernández, L.P. (2004).** Measurement error in waves research laboratorios. Ing Hidráulica en México XIX, pp. 101–106.

23. **Fernández, L.P.S., Hernández, J.J.C., Pérez, L.A.S., Charles, R.H. (2013).** Control Neuronal Combinado para Generar Espectros de Oleajes. Rev. Iberoam. Automática e Informática Ind. RIAI, Vol. 10, pp. 413–422.

24. **Fernández, L.P.S., Charles, R.H., Cárdenas, R.L. (2007).** low-cost wave generation system based on combined neural control and a linear motor. IFAC Proc., Vol. 40, No. 1, 171–176. DOI: 10.3182/2007 0213-3-CU-2913.00029.

25. **Pastor, L., Diaz de León, J.L, Yáñez, C., Herrera, R. (2004).** Cuantificación del error en las mediciones debido a la frecuencia de muestreo [The Error's Quantification in the Measurements due to Sampling Frequency]. Computación y Sistemas, Vol. 8, No. 2, pp. 86–105.

26. **The American Society of Mechanical Engineers (2009).** Standard B46.1-2009: Surface Texture Surface Roughness, Waviness, and Lay. ASME.

27. **Fernandez, L.P.S., Perez, L.A.S., Hernandez, J.J.C., de-Rodriguez, J., Jordan, G. (2018).** Biomechanical Signal Analysis for Evaluation of

Gait in Parkinson's Disease. IEEE 23rd International Conference on Emerging Technologies and Factory Automation (ETFA), pp. 792–799. DOI: 10.1109/ETFA.2018.8502581.

28. **Thomson-Richard, E., Emery, W.J. (2014).** Data analysis methods in physical oceanography. Elsevier.

29. **Koop, M.M., Shivitz, N., Brontë-Stewart, H. (2008).** Quantitative measures of fine motor, limb, and postural bradykinesia in very early stage. Untreated Parkinson's Disease Mov Disord, Vol. 23, 1262–1268. DOI: 10.1002/mds.22077.

30. **Stansell, P., Wolfram, J., Linfoot, B**. **(2002).** Effect of sampling rate on wave height statistics. Ocean Engineering, Vol. 29, No. 9, pp. DOI: 1023–1047.10.1016/S0029-8018(01)00066-X.

31. **Sánchez-Fernández, L.P. (2004).** Interpolation with splines and FFT in wave signals. Res. Comput. Sci., Vol. 10, pp. 387–400.

32. **Kuhlmann, V., Sinton, A., Dewe, M., Arnold, C. (2007).** Effects of sampling rate and adc width on the accuracy of amplitude and phase measurements in power-quality monitoring. IEEE Trans Power Deliv, Vol. 22, No. 2, pp. 758–764. DOI. 10.1109/TPWRD.2007.893389.

33. **Sanchez, L.P., Arteaga, E. (1998).** Dynamic modelling and control schemes for a Rehbock channel. Ing. Hidraul. en Mex. Vol. 13, pp. 5–13.

34. **Fernandez, L.P.S., Perez, L.A.S., Hernandez, J.J.C. (2018).** Biomechanical Signal Analysis for Evaluation of Gait in Parkinson's Disease - IEEE Conference Publication. IEEE 23rd International Conference on Emerging Technologies and Factory Automation (ETFA), pp. 792–799.

35. **Carbajal-Hernández, J.J., Sańchez-Fernández, L.P., Landassuri-Moreno, V.M., De Medel-Juárez, J.J. (2013).** Misalignment identification in induction motors using orbital pattern analysis. Lect. Notes Comput. Sci., Vol. 8259, pp. 50–58. DOI: 10.1007/978-3-642-41827-3_7.

36. **Carbajal-Hernández, J.J., Sánchez-Fernández, L.P., Suárez-Guerra, S., Hernández-Bautista, I. (2014).** Rotor unbalance detection in electrical induction motors using orbital analysis. Lect. Notes Comput. Sci., Vol. 8495, pp. 371–379. DOI: 10.1007/978-3-319-07491-7_38.